81-GT-147

ASME

THE AMERICAN SOCIETY OF MECHANICAL ENGINEERS
345 E 47 St., New York, N.Y. 10017

Component Mode Synthesis of Large Rotor Systems

D. F. Li[1]

E. J. Gunter
Mechanical & Aerospace
Engineering Department
University of Virginia
Charlottesville, Va. 22901

A scheme is presented for calculating the vibrations of large multi-component flexible rotor systems based on the component mode synthesis method. It is shown that, by a modal expansion of the elastic interconnecting elements, the system modal equation can be conveniently constructed from the undamped eigen representations of the component subsystems. The capability of the component mode method is demonstrated in two examples: a transient simulation of a two-spool gas turbine engine equipped with a squeeze-film damper; and an unbalance response analysis of the Space Shuttle Main Engine oxygen turbopump in which the dynamics of the rotor and the housing are both considered.

Introduction

When the total number of degrees of freedom of a dynamic system is too large for even modern digital computers to handle economically, analysts resort to the modal method in which the system is represented by its free vibration modes. The advantage of using a modal representation consisting of a few low frequency modes is that the associated problem size can be reduced, leading to a subsequent saving in computer time [1-12]. The modal method has been a popular tool in solving difficult problems involving single and double spool rotors. Childs [1-2, 4-5] performed transient rotor-dynamic analyses with undamped normal modes. Choy [6, 8] and Gunter, et al. [7] evaluated the accuracy of the modal method in single-shaft linear rotor analysis including bowed shaft and skewed disk effects. Transient analyses of dual-rotor aircraft engines were attempted by Dennis, et al. [3] and Childs [4]. In both papers, the transient orbits of the rotors due to suddenly applied unbalance were computed with the undamped normal modes of the linearized system. In [4], rotor viscous destabilizing internal damping was accounted for by judiciously applying anti-symmetric, cross-coupled stiffness factors to the modal equations. In all these analyses, the system modal equation was based on normal modes calculated from the full equation of motion of the complete system.

A more advanced form of the normal mode method is offered in the use of component modes [9-11]. In this scheme, a dynamic structure is partitioned into a number of smaller substructures. Each substructure modal character is individually derived, through analytical means or actual vibration testing [12]. The total structure is then constructed from a reduced number of component modes from each substructure. This procedure, besides having the benefit of representing thousands of degrees of freedom by only a handful of normal modes, also allows one to build a sound analytical model because each substructure can be conveniently checked for accuracy before assembly. Furthermore, equation size that the computer has to handle at one time can be further reduced, and the type of interface between the substrucures can be altered without having to recalculate a new set of modal coordinates. Component mode synthesis is used extensively in the aerospace industry for the calculation of the undamped natural frequencies of large airframe structures. Hurty [9] and Craig, et al. [10] are among the earlier investigators. A summary on component mode analysis was presented by Hou [11]. Experimental extraction of undamped modes and the use of a "building block" approach were investigated by Klosterman [12]. In most applications, the substructures are required to share common degrees of freedom at the interconnections of the substructures. Therefore, a set of constraint equations is necessary to determine a reduced modal equation of motion. In rotor systems, a similar but different problem is usually encountered. Interface between substructures consists of bearings, seals, and flexible supports that are themselves elastic. When there is no common degree of freedom being shared by the substructures, flexible connections can be introduced simply as generalized damping, stiffness, and forces into the modal equations. This procedure is exemplified in the analysis of a linear rotor-casing system using undamped modes [5]. Childs started with two sets of casing modes in the two asymmetric planes. Together with the rotor free-free modes, the undamped modes of the rotor-casing system (i.e. the free vibration modes of the total system) were obtained using component mode synthesis. The system modes were then used to develop the system modal equations with the added damping. The total number of generalized coordinates is equal to the number of undamped component modes originally used.

In this paper, a systematic approach to establish the modal equation of motion from component modes is presented. Here, it is built directly from the component modes of the

[1] Now at the General Motors Research Laboratories, Mechanical Research Department, Warren, Michigan 48090.

Contributed by the Gas Turbine Division for presentation at the International Gas Turbine Conference and Products Show, Houston, Texas, March 9-12, 1981 of THE AMERICAN SOCIETY OF MECHANICAL ENGINEERS. Manuscript received at ASME Headquarters December 15, 1980. Paper No. 81-GT-147.

Copies will be available until December 1981.

substructures; therefore, the extra step involved in computing the system undamped mode (as it is done in [5]) is eliminated. The scheme is completely general and not limited to any fixed system configuration.

Theory

A component mode analysis starts with dividing the system into a number of substructures or subsystems. There is generally no constraint on how large a portion of the total system that each subsystem represents. For example, a subsystem may include all possible degrees of freedom in a rotor shaft. Alternatively, the same rotor may also be represented by three subsystems: one for the coordinates in the two lateral planes, one for torsion, and one for axial vibration. The undamped orthonormal mode shapes and eigenvalues of each subsystem are obtained by omitting all interconnecting elements and damping. (The associated eigenvalue problem may be solved by the transfer matrix method for all rotors and beam-like structures. More complicated structures may be treated by the finite element method.)

For a subsystem consisting of a linearly elastic nonrotating structure, the stiffness matrix is always symmetrical. The eigenvalue problem is

$$[M_x]\{\ddot{x}\} + [\tilde{K}_s]\{x\} = \{0\} \tag{1}$$

and the orthogonality may be expressed as

$$[\phi]^T[M_x][\phi] = [\underline{I}] \tag{2}$$

$$[\phi]^T[\tilde{K}_s][\phi] = [\underline{\omega_s}^2] \tag{3}$$

And for a subsystem consisting of a rotor, the stiffness matrix is generally asymmetrical due to internal friction and asymmetric bearing stiffness. The usual approach is to separate it into a symmetric part and an asymmetric part [5-7]. Only the symmetric stiffness part is used in the evaluation of the undamped component modes. The asymmetric part is added to the modal equations at a later stage. Following this approach, one has the choice of either the free-free rotor modes, containing the shaft stiffness alone, or the rotor-bearing modes, containing both the shaft stiffness and the principal bearing stiffnesses. In the first case, the eigenvalue problem for the free-free rotor modes has the same form as in equations (1) to (3). In the second case, identical modal characteristics are used in both lateral planes to minimize the amount of computations. Hence, the mean bearing stiffness in the lateral directions is considered; the eigenvalue problem becomes:

$$[M_x]\{\ddot{x}\} + \left[[K_s] + \frac{[\underline{K_{xx}}] + [\underline{K_{yy}}]}{2}\right]\{x\} = \{0\} \tag{4}$$

with the orthogonality,

$$[\phi]^T[M_x][\phi] = [\underline{I}] \tag{5}$$

$$[\phi]^T[K_s][\phi] + \frac{[\phi]^T[[\underline{K_{xx}}] + [\underline{K_{yy}}]][\phi]}{2} = [\underline{\omega_p}^2] \tag{6}$$

The modal transformation for the rotor in the lateral planes is therefore given by,

Nomenclature

e = viscous damping coefficient (T)
e_u = unbalance eccentricity
J_p, J_T = polar moment and transverse moment of inertia of a disk (ML^2)
Re[ ] = real part of the complex quantity in [ ]
X, Y, x, y = lateral displacements (L)
$\dot{x}, \dot{y}$ = velocities in x and y directions (L/T)
$\ddot{x}, \ddot{y}$ = accelerations in x and y directions (L/T^2)
Z, z = axial displacement (L)
α, β = phase angle of unbalance in lateral and rotational coordinates
ϵ = dry friction loss angle
θ = rotating coordinate with vector in the Y direction
ϕ = rotating coordinate with vector in the $-X$ direction
τ = disk skew angle
ζ_s = viscous modal damping ratio
ψ = torsional coordinate with vector in the Z-direction
ω = frequency of harmonic vibration (1/T)
Ω = rotor spin speed (1/T)
$\dot{\Omega}$ = rotor acceleration ($1/T^2$)

Matrices

$[C]$ = system damping matrix
$[C_{xx}], [C_{yy}], [C_{x\theta}]$ . . . etc = bearing damping matrices
$[c]$ = modal damping matrix
$[\bar{c}]^{(ij)}$ = modal damping due to interconnections
$[\underline{J_t}], [\underline{J_p}]$ = transverse and polar moment of inertia
$[\underline{I}]$ = unity matrix
$[\tilde{K}]$ = system stiffness matrix
$[K_{xx}], [K_{yy}], [K_{x\theta}]$, . . . etc = bearing stiffness matrices
$[\bar{K}]$ = symmetric stiffness matrix
$[k]$ = modal stiffness matrix
$[\bar{k}]^{(ij)}$ = modal stiffness due to interconnection
$[M]$ = system mass matrix
$[m]$ = modal mass matrix
$[0]$ = zero matrix
$\{q^{(i)}\}$ = generalized coordinates in subsystem i
$\{q\}, \{\dot{q}\}, \{\ddot{q}\}$ = generalized displacement, velocity, and acceleration vectors
$[\phi]$ = orthonormal eigenvector matrix
$[\underline{\omega_s^2}]$ = undamped eigenvalue diagonal matrix for rotor free-free modes or structural modes
$[\underline{\omega_p^2}]$ = undamped eigenvalue diagonal matrix for rotor modes including bearing stiffness
$[\underline{\ }]$ = indicates diagonal matrix
$[\ ]^T$ = transpose of matrix [ ].
$\Delta[\ ], \Delta\{\ \}$ = small increment in matrix [ ] and { }

$$\begin{Bmatrix} \{x\} \\ \\ \{y\} \end{Bmatrix} = \begin{bmatrix} [\phi] & [0] \\ \\ [0] & [\phi] \end{bmatrix} \begin{Bmatrix} \{q_x\} \\ \\ \{q_y\} \end{Bmatrix} \tag{7}$$

The shaft flexural stiffness is now implicit in the mode shape and conveniently expressed by the eigenvalues. Axial and torsional vibrations of the shaft that are not coupled to the lateral shaft motion may be treated by equations (1) to (3) and added to equation (7) in the generalized coordinates.

Assembly of Modal Equation. A global model equation consisting of w subsystems is shown below.

$$\begin{bmatrix} [I] & [0] & . & . & . \\ [0] & [I] & . & . & . \\ . & . & . & . & . \\ . & . & . & [I] & [0] \\ . & . & . & [0] & [I] \end{bmatrix} \begin{Bmatrix} \{\ddot{q}^{(1)}\} \\ \{\ddot{q}^{(2)}\} \\ . \\ \{\ddot{q}^{(w-1)}\} \\ \{\ddot{q}^{(w)}\} \end{Bmatrix}$$

$$+ \begin{bmatrix} [c]^{(11)} & [c]^{(12)} & . & . & . \\ [c]^{(21)} & [c]^{(22)} & . & . & . \\ . & . & . & . & . \\ . & . & . & [c]^{(w-1,w-1)} & [c]^{(w-1,w)} \\ . & . & . & [c]^{(w,w-1)} & [c]^{(w,w)} \end{bmatrix} \begin{Bmatrix} \{\dot{q}^{(1)}\} \\ \{\dot{q}^{(2)}\} \\ . \\ \{\dot{q}^{(w-1)}\} \\ \{\dot{q}^{(w)}\} \end{Bmatrix}$$

$$+ \begin{bmatrix} [k]^{(11)} & [k]^{(12)} & . & . \\ [k]^{(21)} & [k]^{(22)} & . & . \\ . & . & . & . \\ . & . & [k]^{(w-1,w-1)} & [k]^{(w-1,w)} \\ . & . & [k]^{(w,w-1)} & [k]^{(w,w)} \end{bmatrix} \begin{Bmatrix} \{q^{(1)}\} \\ \{q^{(2)}\} \\ . \\ \{q^{(w-1)}\} \\ \{q^{(w)}\} \end{Bmatrix} = \begin{Bmatrix} \{f^{(1)}\} \\ \{f^{(2)}\} \\ . \\ \{f^{(w-1)}\} \\ \{f^{(w)}\} \end{Bmatrix} \tag{8}$$

The above equation has been partitioned into submatrices. Each of the diagonal submatrices is square and has the dimension equal to the number of normal modes employed in the corresponding subsystem. The off-diagonal matrices represent the coupling of the subsystems due to the interconnecting elements. The stiffness and damping submatrices in equation (8) can be expressed as the summations of two terms:

$$[k]^{(ij)} = \delta_{ij}[\omega^2]^{(ii)} + [\bar{k}]^{(ij)} \tag{9}$$

$$[c]^{(ij)} = \delta_{ij}[d]^{(ii)} + [\bar{c}\,]^{(ij)} \tag{10}$$

where

$$\delta_{ij} = \begin{cases} 0\ , & i \neq j \\ 1\ , & i = j \end{cases} \tag{11}$$

The first matrix on the right hand side of equations (9-10) for a nonrotating flexible structure is determined by the subsystem eigenvalues (equations (3, 6)) and the associated structural modal damping,

$$[\omega^2]^{(ii)} = [\omega_s^{\,2}]^{(ii)} \tag{12}$$

$$[d]^{(ii)} = [2\zeta_s\omega_s]^{(ii)\,2} \tag{13}$$

and for a flexible rotor (treated as a subsystem containing both lateral planes),

$$[\omega^2]^{(ii)} = \begin{bmatrix} a[\omega_A{}^2] & b[\omega_A{}^2] \\ \\ -b[\omega_A{}^2] & a[\omega_A{}^2] \end{bmatrix} + \begin{bmatrix} [\omega_B{}^2] & [0] \\ \\ [0] & [\omega_B{}^2] \end{bmatrix} \tag{14}$$

$$[d]^{(ii)} = e \begin{bmatrix} [\omega_A{}^2] & [0] \\ \\ [0] & [\omega_A{}^2] \end{bmatrix} \tag{15}$$

where

$$a = \frac{1}{\sqrt{1+\epsilon^2}} \tag{16}$$

$$b = a\epsilon + e\Omega \tag{17}$$

The effects of internal friction are represented in the above equations by the dry friction loss angle ϵ and the viscous friction coefficient e (see Appendix). When the free-free shaft modes are used, $[\omega_A{}^2]$ and $[\omega_B{}^2]$ in equations (14-15) are defined by

$$[\omega_A{}^2] = [\omega_s^{\,2}] \text{ (in equation (3))} \tag{18}$$

$$[\omega_B{}^2] = [0] \tag{19}$$

Otherwise, when the bearing stiffness is included in the normal modes (as in equation (4)), they become:

$$[\omega_A{}^2] = [\omega_{-p}{}^2] - [\omega_B{}^2] \tag{20}$$

$$[\omega_B{}^2] = \frac{[\phi]^T[[K_{xx}] + [K_{yy}]][\phi]}{2} \tag{21}$$

The linearly elastic elements omitted in the undamped mode calculation contribute to the coupling matrices $[k]^{(ij)}$ and $[c]^{(ij)}$ in the second term of equations (9-10). Typically, these elements consist of the bearing stiffness and damping, gyroscopic moments, and rotor acceleration. To aid in forming $[k]^{(ij)}$ and $[c]^{(ij)}$, it is advantageous to assign a number to

[2] The viscous damping ratio ζ_s for each mode is related to the viscous damping coefficient by $\zeta_s = e\,\omega_s/2$.

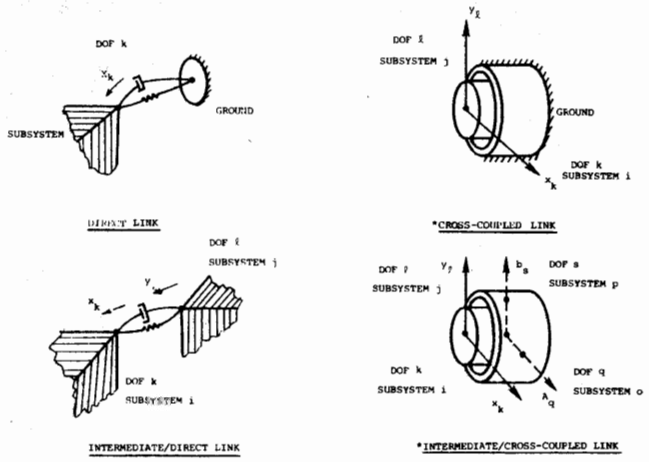

Fig. 1 Linearly elastic connection types in component mode synthesis (* Figures show $l=j$ and $o=p$)

every DOF (degree of freedom) in each subsystem. Modal expansion matrices are used to establish the equivalence of the elastic elements in the modal coordinates. A linear element connecting the k^{th} degree of freedom in subsystem i and the ℓ^{th} degree of freedom in subsystem j has the following modal expansion.

$$[\Gamma]_{\substack{k\ell \\ m\times n}}^{(ij)} = \{\phi_{k1}^{(i)}\phi_{k2}^{(i)}\ldots\ldots \phi_{km}^{(i)}\}^T\{\phi_{\ell 1}^{(j)}\phi_{\ell 2}^{(j)}\ldots\ldots\phi_{\ell n}^{(j)}\} \tag{22}$$

where

$\phi_{rs}^{(f)}$ = deflection at the r^{th} degree of freedom in the s^{th} mode of subsystem f

m,n = number of modes used in the subsystem i and subsystem j respectively.

All linearly elastic elements may be generalized into four distinct linking types (or combinations of these types) as illustrated in Fig. 1. Each link consists of a stiffness coefficient K and a damping coefficient C.

Direct Link. This link represents a linear element connecting the k^{th} DOF in the i^{th} subsystem to the stationary ground. The contributions in the modal stiffness and damping are:

$$\underset{m\times m}{\Delta[\bar{k}]}^{(ii)} = K[\Gamma]_{kk}^{(ii)} \tag{23}$$

$$\underset{m\times m}{\Delta[\bar{c}]}^{(ii)} = C[\Gamma]_{kk}^{(ii)} \tag{24}$$

Cross-Coupled Link. In this link, a coupling force is induced at the k^{th} DOF in the i^{th} subsystem by the motion at the ℓ^{th} DOF in the j^{th} subsystem. This type of link can be found in dynamic components involving a fluid (e.g. fluid-film bearing). The modal contribution consists of:

$$\underset{m\times n}{\Delta[\bar{k}]}^{(ij)} = K[\Gamma]_{k\ell}^{(ij)} \tag{25}$$

$$\underset{m\times n}{\Delta[\bar{c}]}^{(ij)} = C[\Gamma]_{k\ell}^{(ij)} \tag{26}$$

Intermediate/Direct Link. This link consists of an elastic element interconnected between the k^{th} DOF in the i^{th} subsystem and the ℓ^{th} DOF in the j^{th} subsystem. The contribution to model stiffness is:

$$\underset{m\times m}{\Delta[\bar{k}]}^{(ii)} = K[\Gamma]_{kk}^{(ii)} \tag{27}$$

$$\underset{n\times n}{\Delta[\bar{k}]}^{(jj)} = K[\Gamma]_{\ell\ell}^{(jj)} \tag{28}$$

$$\underset{m\times n}{\Delta[\bar{k}]}^{(ij)} = -K[\Gamma]_{k\ell}^{(ij)} \tag{29}$$

$$\underset{n\times m}{\Delta[\bar{k}]}^{(ji)} = -K[\Gamma]_{\ell k}^{(ji)} = \left[\Delta[\bar{k}]^{(ij)}\right]^T \tag{30}$$

The contribution to modal damping is computed by replacing $[k]$ by $[c]$ and K by C in the above expressions.

Intermediate/Cross-Coupled Link. In this link, equal and opposite forces are developed at the ℓ^{th} DOF in the j^{th} subsystem and the s^{th} DOF in the p^{th} subsystem due to the coupling effect of the relative motion between the k^{th} DOF in the i^{th} subsystem and the q^{th} DOF in the o^{th} subsystem. It is equivalent to a cross-coupled link connecting two pairs of DOFs. An example of this is the cross-coupled dynamic coefficient of a journal bearing installed intermediately between two concentric rotating shafts. The stiffness K contributes to:

$$\underset{n\times m}{\Delta[\bar{k}]}^{(ji)} = K[\Gamma]_{\ell k}^{(ji)} \tag{31}$$

$$\underset{u\times t}{\Delta[\bar{k}]}^{(po)} = K[\Gamma]_{sq}^{(po)} \tag{32}$$

$$\underset{n\times t}{\Delta[\bar{k}]}^{(jo)} = -K[\Gamma]_{\ell q}^{(jo)} \tag{33}$$

$$\underset{u\times m}{\Delta[\bar{k}]}^{(pi)} = -K[\Gamma]_{sk}^{(pi)} \tag{34}$$

Again, similar expressions are applicable for computing the contribution due to damping by replacing K with C in the above equations.

The total effect due to linearly linking elements is the sum of all the individual contributions. (For example, a fluid-film bearing mounted in a rigid housing is representable by two direct links, and two cross-coupled links between the shaft and the ground.)

The gyroscopic forces associated with a rotor represent additional modal contributions. This is dealt with in a similar manner using modal expansion. For each pair of angle DOFs, k^{th} DOF in subsystem i and ℓ^{th} DOF in subsystem j, that has polar moment of inertia along the rotor axis,

$$\underset{m\times n}{\Delta[k]}^{(ij)} = \frac{\dot{\Omega}J_P}{2}[\Gamma]_{k\ell}^{(ij)} \tag{35}$$

$$\underset{n\times m}{\Delta[k]}^{(ji)} = \frac{-\dot{\Omega}J_p}{2}[\Gamma]_{\ell k}^{(ji)} = -\left[\Delta[k]^{(ij)}\right]^T \tag{36}$$

$$\underset{m\times n}{\Delta[c]}^{(ij)} = \Omega J_p[\Gamma]_{k\ell}^{(ij)} \tag{37}$$

$$\underset{n\times m}{\Delta[c]}^{(ji)} = -\Omega J_p[\Gamma]_{\ell k}^{(ji)} = -\left[\Delta[c]^{(ij)}\right]^T \tag{38}$$

Normally, the cross-coupling is between the θ DOF and ϕ DOF (see Appendix) in the same subsystem such that $i = j$. (An exception is when vibrations in the x-z and y-z planes are treated as separate subsystems.)

Finally, summing up all the foregoing modal contributions, the second term of the modal stiffness matrix in equation (9) for $i, j = 1$ to w is:

$$[k]^{(ij)} = \sum_{\substack{\text{over all}\\ \text{elastic}\\ \text{links}}}^{\text{sum}} \Delta[\bar{k}]^{(ij)} + \sum_{\substack{\text{over all}\\ \text{gyroscopic}\\ \text{links}}}^{\text{sum}} \Delta[\bar{k}]^{(ij)} \tag{39}$$

The corresponding damping matrix in equation (10) is obtained by replacing $[\bar{k}]^{(ij)}$ by $[\bar{c}]^{(ij)}$ in the above equation.

Modal forces are related to the actual forces acting at the nodes according to the mode shapes. For a forcing function F existing at the k^{th} DOF in the i^{th} subsystem, the resulting modal forces are

$$\underset{m\times 1}{\Delta\{f^{(i)}\}} = \{\phi_{k1}^{(i)}\phi_{k2}^{(i)}\ldots\phi_{km}^{(i)}\}^T F \tag{40}$$

This expression is used to expand concentrated forces due to unbalance, disk skew, or nonlinear forces at any of the nodal degrees of freedom. The real displacement at the k^{th} DOF in the i^{th} subsystem at any given time is:

$$x_k^{(i)} = \{\phi_{k1}^{(i)}\ \phi_{k2}^{(i)} \ldots \phi_{km}^{(i)}\}\ \{q^{(i)}\} \tag{41}$$

Hence, it is shown that the governing equation of a complex rotor system may be expressed in the generalized coordinates by adding up the contributions of all the linearly flexible links to the basic uncoupled modal equation. Once the governing equation is established, critical speeds, stability, forced or transient responses may be solved in the modal coordinates. The final results can be transformed back into real coordinates by equation (41). Note that in nonlinear transient analyses, it is usually necessary to transform back and forth between the real and the modal coordinates during computation of the nonlinear forces.

Applications

The theory is applied to two high-speed turbomachines; (1) a two-spool aircraft gas turbine engine, (2) Space Shuttle Main Engine liquid oxygen turbopump (SSME HPOTP).

Two-Spool Aircraft Engine

Figure 2 represents a computer model of the two-spool gas turbine engine. The engine consists of an inner core rotor called the power turbine, which is supported by two main bearings located at the shaft extremities. There are two intermediate differential bearings (FDB and ADB) connecting the power turbine to the gas generator rotor. The gas generator is supported principally by four bearings. In this engine design, a squeeze-film damper bearing is incorporated at the No. 3 bearing location to reduce turbine vibration amplitudes and bearing forces.

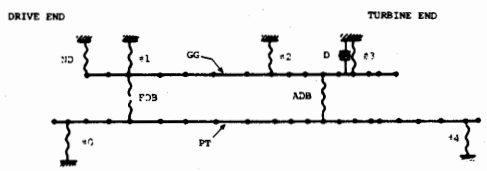

Fig. 2 Two-spool aircraft turbine engine lumped parameter computer model (*PT* - power turbine rotor, *GG* - gas generator rotor, *FDB* - front differential bearing, *ADB* - aft differential bearing, *D* - damper bearing)

The model, which has a total of 38 nodes and 152 degrees of freedom, is considered as being composed of two subsystems; namely, the gas generator rotor, and the power turbine rotor. The component modes of the rotors are obtained independently of each other by omitting the effects of disk gyroscopics, the squeeze-film damper, and the two intershaft bearings. To keep the computer time requirement within reasonable limits, a total of 12 component modes containing two gas generator component modes and four power turbine component modes in each lateral plane are used. This includes all undamped component modes that are below 500 Hz (30,000 cycles per minute (CPM)).

The first part of this application is to compute the transient response of the gas turbine due to a suddenly applied unbalance in the power turbine rotor under steady-speed operation. The gas generator is taken to be balanced and operating at 1571 rad/s (15,000 r/min). The power turbine is operating steadily at 1780 rad/s (17,000 r/min) with zero vibration level when an unbalance distribution is imposed. This particular unbalance consists of 25 g cm each at the second stage turbine and at the rotor mid-span at π rad (180 deg) apart from each other. In this case, the system is assumed to be linear. Figure 3 shows the orbits observed at the second stage gas generator turbine for the first 10 and the last 15 cycles in a total of 40 cycles of simulation. Although the steady-state orbit is not yet completely developed after 40 cycles, the magnitude and the phase angle of the vibration are quite established. A comparison of this result with an independent steady-state response calculation has indicated excellent correlation. The maximum response amplitude observed during the initial transient motion is about two times the size of the steady-state orbit.

Due to the use of an improperly designed damper, a nonlinear "jump" was observed in the gas generator vibration during engine tests. A study is presented here in which the jump phenomena is simulated. The squeeze-film damper has a length of 11 mm, a diameter of 129 mm, and a radial clearance of 0.1 mm. A retainer spring of 2.15×10^7 N/m is used to center the outer raceway of the rolling element bearing inside the damper. The diaphragm which supports the squeeze-film damper bearing is taken to be rigid. The bearing force is calculated with the short bearing theory in the simulation. The power turbine rotor is assumed to be

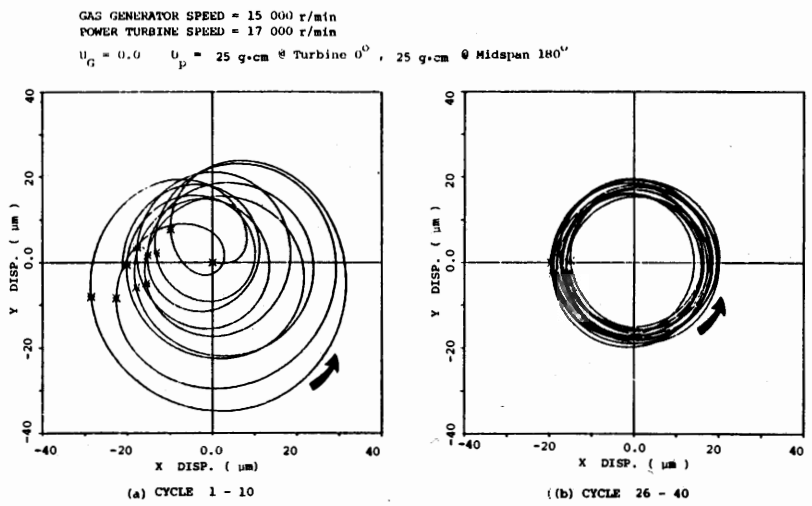

Fig. 3 Linear transient orbits of the gas generator second stage turbine due to coupled power turbine unbalance (→ direction of rotor precession)

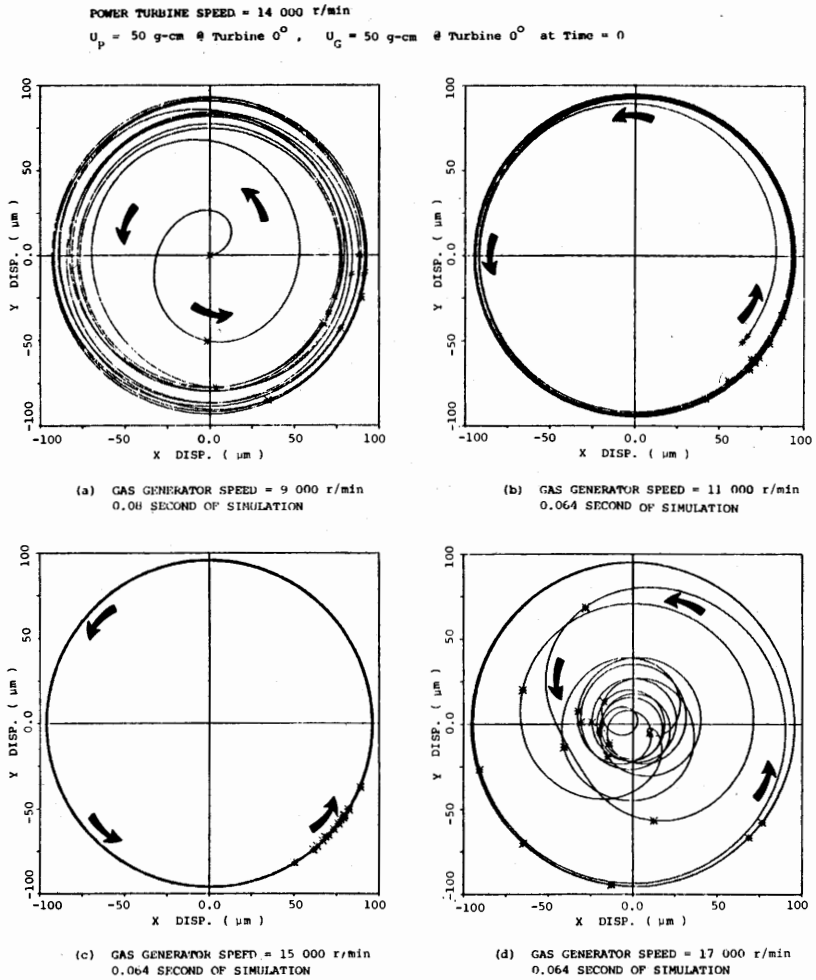

Fig. 4 Nonlinear transient rotor orbits at squeeze film damper bearing showing nonlinear jump (→ direction of rotor precession)

operating at 1466 rad/s (14,000 r/min) with an unbalance of 50 g cm at the turbine end. The gas generator rotor has 50 g cm of unbalance at the second stage turbine.

The gas generator rotor speed is increased from 943 rad/s (9000 r/min) in steps of 209 rad/s (2000 r/min) until the jump phenomena occurs. At 943 rad/s (9000 r/min), the transient motion is started initially at zero displacement and velocity. For each speed, the nonlinear transient is calculated for about 10 gas generator rotor revolutions. The starting conditions at rotor speeds other than the initial speed of 943 rad/s (9000 r/min) are taken to be equal to the final displacement and velocity computed at the end of the simulation cycles for the previous gas generator speed.

Figure 4 represents the transient orbits of the gas generator rotor at the damper location as the gas generator is brought up in speed until the jump phenomena occur. The initial transient rotor motion at 943 rad/s (9000 r/min) is shown in Fig. 4(*a*). The orbits are calculated for about 11 gas generator rotor revolutions after it is released with zero velocity from the bearing center. The timing mark is synchronized with the unbalance vector in the gas generator and is shown as an asterisk at the end of each gas generator rotor revolution. Because the rotors are operating at different speeds, the unbalance forces have two frequency components. Therefore, a response pattern repeating itself for every revolution is not observed even when the system has reached steady-state operation.

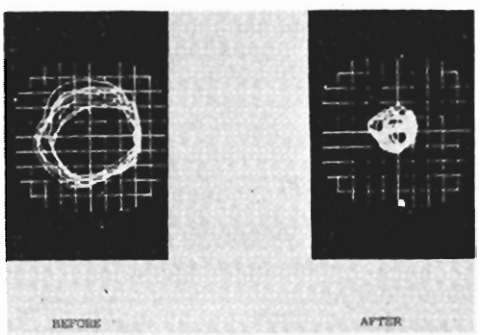

Fig. 5 Experimental gas turbine engine casing vibration orbits before and after nonlinear jump phenomena [13]

Figure 4(*b*) shows the nonlinear rotor motion at the damper location at 1152 rad/s (11,000 r/min). Limiting orbits of large amplitude are formed very rapidly in less than one gas generator revolution. The damper is seen to be operating at eccentricities in excess of 0.9 of the radial clearance. A fluctuation of the phase lag angle about 45 deg persists throughout the simulation at this speed. At 1571 rad/s (15,000 r/min), a case of an extremely overloaded damper is observed in Fig. 4(*c*). The rotor appears to orbit in a large circle with an eccentricity ratio of about 0.95.

Finally, Fig 4(*d*) illustrates the nonlinear jump phenomena

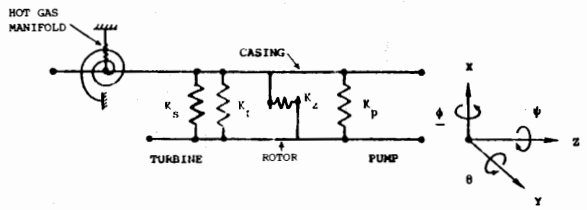

Fig. 6 Space Shuttle Main Engine oxygen pump computer simulation lumped parameter model (K_p - pump bearing, K_z - balance piston, K_t - turbine bearing, K_s - turbine seals)

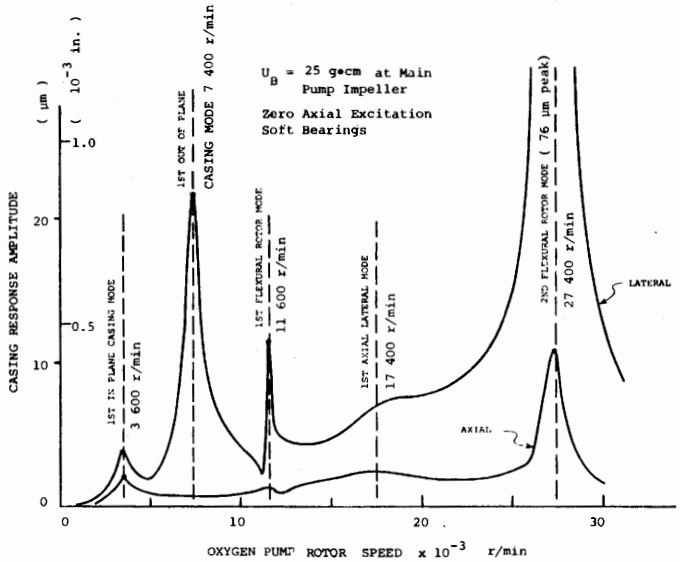

Fig. 7 Lateral and axial steady-state response amplitudes at casing prebumer pump end due to main pump impeller unbalance

at the gas generator speed of 9780 rad/s (17,000 r/min). It is seen that the rotor orbit is reduced to about a quarter of its initial size within five revolutions. The jump in the amplitude is accompanied by a shift of the timing mark to align approximately with the negative x-axis. This phase angle change is important as it indicates that the gas generator rotor has rapidly passed through the critical speed of the gas generator mode due to the sudden reduction in the effective damper stiffness which resulted from a smaller orbit size.

Figure 5 represents the experimentally measured vibration orbits of the engine casing in a test run taken before and after the jump occurs. The appearance of these orbits seems to be similar to those obtained in the transient computer simulation.

Space Shuttle Oxygen Pump

In this application, the linear steady-state unbalance response of the space shuttle oxygen pump is computed. Figure 6 shows a computer model of the oxygen pump assembly. It consists of a single rotating shaft mounted in two pairs of flexibly supported rolling element bearings inside a flexible casing. Due to the flexibility in the hot gas manifold, which serves as the only major casing support, a number of rotor/casing resonsant modes are created.

During the development of the oxygen pump, accelerometers were placed on the pump casing to monitor the radial and axial vibration levels. Due to the limited space available inside the test pump, no proximity probes were installed to measure the rotor motions directly. The lack of a measurement of the rotor shaft amplitudes has made it extremely difficult to determine whether a pump failure oc-

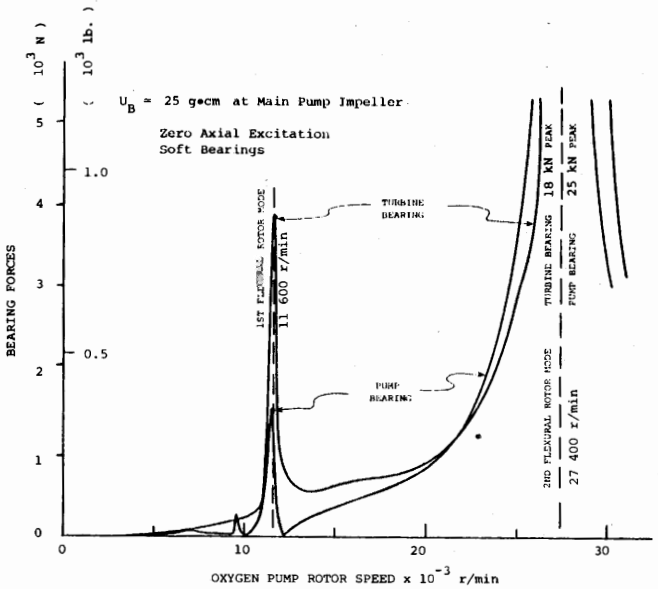

Fig. 8 Bearing forces in the x-direction due to main pump impeller unbalance

curing at about 2618 rad/s (25,000 r/min) was caused by a resonant mode of the rotor or a resonant mode introduced by the flexibly mounted casing. It was intended that the unbalance response analysis would aid in the identification of this failure mode.

The pump is considered to be composed of two subsystems – the casing and the turbopump rotor. Each node in the casing structure is taken to have six degrees of freedom. The casing modes with the hot gas manifold are calculated individually in the x-θ-z lateral axial and the y-$\phi\Psi$ lateral torsional planes. A total of four modes in each plane are included. The frequency of the lowest mode in each plane has been verified by experimental data. The rotor modes are computed using free-free boundary conditions. The highest of the eight modes used at 5672 Hz (340,300 CPM) is more than ten times the full power speed of the turbopump.

In the rotor-flexural mode calculation, the axial and torsional motions are not considered. The axial rotor coordinate is accounted for in the modal analysis by the addition of a rigid body rotor axial mode. Each node in the rotor, therefore, has five degrees of freedom.

In this system, a total of 289 degrees of freedom is represented by 25 generalized coordinates. Five percent modal damping, based on test data, is applied to each of the casing modes. The balance piston has a stiffness of 36.7 ω^2 N/m (0.21 ω^2 lb/in.) and is taken to provide 10 percent of the critical damping in the axial direction. It is assumed that each pair of bearings produces 7.0×10^5 N/m to 1.57×10^6 N/m (0.4×10^6 lb/in. to 0.9×10^6 lb/in.) of stiffness (depending on the rotor speed), and 876 N•s/m (5 lb•s/in) of damping. An unbalance of 25 g cm is placed at the main pump impeller.

Figure 7 represents the calculated casing vibration at the pump end. The vibration modes have been identified in a critical speed calculation according to the proportion of strain energy in the rotor and the pump casing. It can be seen that the highest response amplitude is predicted at the second rotor mode of about 2870 rad/s (27,400 r/min). Axial vibration in this mode is due to the coupling of the axial and lateral forces at the hot gas manifold. The axial-lateral mode at 1822 rad/s (17,400 r/min) does not appear to be particularly sensitive to this unbalance.

The computed forces transmitted to the bearings are presented in Fig. 8. A serious threat to the safety of the pump

is uncovered at the second rotor critical speed where the magnitudes of the forces increase to as high as 25 kN (5600 lb.). Vibrations due to casing flexibility, although readily detected on the casing, do not generate much forces at the bearings.

The result in this analysis indicates that the second rotor mode is a potential danger to the operation of the oxygen pump and could have been responsible for the vibration problem encountered in the test pump. Further testings are now underway to examine this possibility.

Summary and Conclusions

A procedure was developed for the dynamic analysis of large flexible rotor systems with the component mode method. This procedure does not restrict the form of the rotor model. Yet it keeps the size of the governing equation manageable. Because a large system can be divided into a number of much simpler subsystems, the representative component modes can be easily and accurately computed. If desired, these modal informations may be verified by experimental testing.

A two-spool aircraft gas turbine engine equipped with a squeeze film damper bearing and the Space Shuttle Main Engine oxygen turbopump were used to illustrate the capability and versatility of the component mode method. In particular, a transient vibration simulation of the aircraft engine and an unbalance response analysis of the turbopump were presented. The results in both applications were generated by a master computer program. This program has been successfully employed for analyzing the stability, the synchronous response, and the transient response of generally connected multi-component systems.

Acknowledgments

This work is supported in part by the following grants.

NASA - NAS8-31951-5
NASA Lewis - NSG-3177
ARMY - DAG 29-77-C-009

Gratitude is extended to L. E. Barrett of the University of Virginia for providing the damper bearing data and to A. O. DeHart of the General Motors Research Laboratories for reviewing the manuscript.

References

1 Childs, D. W., "A Rotor-Fixed Modal Simulation Model for Flexible Rotating Equipment," ASME *Journal of Engineering for Industry*, Vol. 96, No. 2, 1974, pp. 359-669.

2 Childs, D. W., "Two Jeffcott-Based Modal Simulation Models for Flexible Rotating Equipment," ASME *Journal of Engineering for Industry*, Vol. 97, No. 3, 1975, pp. 1000-1014.

3 Dennis, A. J., Erikson, R. H., and Seitelman, L. H., "Transient Response Analysis of Damped Rotor Systems by the Normal Mode Method," ASME Paper No. 75-GT-58, Gas Turbine Conference, Houston, Texas, March 1975.

4 Childs, D. W., "A Modal Transient Rotor Dynamic Model for Dual-Rotor Jet Engine Systems," ASME *Journal of Engineering for Industry*, Vol. 98, No. 3, 1976, pp. 876-882.

5 Childs, D. W., "The Space Shuttle Main Engine High-Pressure Fuel Turbopump Rotor - Dynamic Instability Problem," ASME JOURNAL OF ENGINEERING FOR POWER, Vol. 100, No. 1, 1978, pp. 48-57.

6 Choy, K. C., *Dynamic Analysis of Flexible Rotor-Bearing Systems Using a Modal Approach*, Ph.D. thesis, University of Virginia, 1977.

7 Gunter, E. J., Choy, K. C., and Allaire, P. E., "Modal Analysis of Turborotors Using Planar Modes - Theory," *Journal of Franklin Institute*, Vol. 305, No. 4, pp. 221-243.

8 Choy, K. C., Gunter, E. J., and Allaire, P. E., "Fast Fourier Transform Analysis of Rotor-Bearing Systems," *Topics in Fluid Film Bearing and Rotor Bearing System Design and Optimization*, presented at the ASME Design Engineering Conference and Shows, Illinois, Apr. 1978.

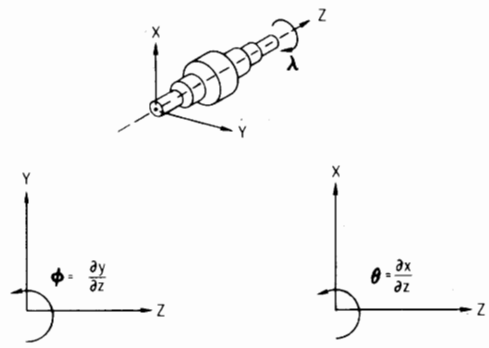

Fig. 9 Rotor coordinates

9 Hurty, W. C., "Dynamic Analysis of Structural Systems Using Component Modes," *AIAA Journal*, Vol. 3, No. 4, Apr. 1965, pp. 678-685.

10 Craig, R. R., and Bampton, M. C. C., "Coupling of Substructures for Dynamic Analysis," *AIAA Journal*, Vol 6, No. 7, July 1968, pp. 1313-1319.

11 Hou, Shou-nien, "Review of Modal Synthesis Techniques and a New Approach," *Shock and Vibration Bulletin 40*, Pt. 4, 1969, pp. 25-39.

12 Klosterman, A. L., *On the Experimental Determination and Use of Modal Representations of Dynamic Characteristics*, Ph.D. dissertation, University of Cincinnati, 1971.

13 Gunter, E. J., Barrett, L. E., and Allaire, P. E., "Design of Nonlinear Squeeze-Film Dampers for Aircraft Engines," ASME *Journal of Lubrication Technology*, Vol. 99, No. 1, 1977, pp. 57-64.

14 D. F. Li, *Dynamic Analysis of Complex Multi-Level Flexible Rotor Systems*, Ph.D. dissertation, University of Virginia, 1978.

APPENDIX

The equation of motion for a rotor [14] is stated without derivation here. The coordinate system for this rotor is shown in Fig. 9. Axial and torsional motion in the z direction are excluded. The effect of internal friction has been added to the governing equation from [7-8]. Forces due to unbalance, disk skew, and rotor acceleration are included in this formulation.

$$\begin{bmatrix} [M_x] & [0] \\ [0] & [M_y] \end{bmatrix} \begin{Bmatrix} \{\ddot{x}\} \\ \{\ddot{y}\} \end{Bmatrix} + \begin{bmatrix} [C_{xx}] & [C_{xy}] \\ [C_{yx}] & [C_{yy}] \end{bmatrix} \begin{Bmatrix} \{\dot{x}\} \\ \{\dot{y}\} \end{Bmatrix} + \begin{bmatrix} [K_{xx}] & [K_{xy}] \\ [K_{yx}] & [K_{yy}] \end{bmatrix} \begin{Bmatrix} \{x\} \\ \{x\} \end{Bmatrix} = \begin{Bmatrix} \{F_x\} \\ \{F_y\} \end{Bmatrix} \tag{42}$$

where

$$[M_x] = [M_y] = \begin{bmatrix} [\underline{M}] & [0] \\ [0] & [J_{\underline{T}}] \end{bmatrix} \tag{43}$$

$$[C_{xx}] = \begin{bmatrix} [C_{\underline{xx}}] & [C_{\underline{x\theta}}] \\ [C_{\underline{\theta x}}] & [C_{\underline{\theta\theta}}] \end{bmatrix} + e[\tilde{K}_s] \tag{44}$$

$$[C_{yy}] = \begin{bmatrix} [C_{\underline{yy}}] & [C_{\underline{y\phi}}] \\ [C_{\underline{\phi y}}] & [C_{\underline{\phi\phi}}] \end{bmatrix} + e[\tilde{K}_s] \tag{45}$$

$$[C_{xy}] = \begin{bmatrix} [C_{\underline{xy}}] & [C_{\underline{x\phi}}] \\ [C_{\underline{\theta y}}] & [C_{\underline{\theta\phi}}] \end{bmatrix} + \Omega \begin{bmatrix} [0] & [0] \\ [0] & [J_P] \end{bmatrix} \tag{46}$$

$$[C_{yx}] = \begin{bmatrix} [C_{\underline{yx}}] & [C_{\underline{y\theta}}] \\ [C_{\underline{\phi x}}] & [C_{\underline{\phi\theta}}] \end{bmatrix} - \Omega \begin{bmatrix} [0] & [0] \\ [0] & [J_P] \end{bmatrix} \tag{47}$$

$$[K_{xx}] = \begin{bmatrix} [K_{\underline{xx}}] & [K_{\underline{x\theta}}] \\ [K_{\underline{\theta x}}] & [K_{\underline{\theta\theta}}] \end{bmatrix} + \frac{1}{\sqrt{1+\epsilon^2}} [\tilde{K}_s] \quad (48)$$

$$[K_{yy}] = \begin{bmatrix} [K_{\underline{yy}}] & [K_{\underline{y\phi}}] \\ [K_{\underline{\phi y}}] & [K_{\underline{\phi\phi}}] \end{bmatrix} + \frac{1}{\sqrt{1+\epsilon^2}} [\tilde{K}_s] \quad (49)$$

$$[K_{xy}] = \begin{bmatrix} [K_{\underline{xy}}] & [K_{\underline{x\phi}}] \\ [K_{\underline{\theta y}}] & [K_{\underline{\theta\phi}}] \end{bmatrix} + \left(\frac{\epsilon}{\sqrt{1+\epsilon^2}} + e\Omega \right) [\tilde{K}_s] + \frac{\dot{\Omega}}{2} \begin{bmatrix} [0] & [0] \\ [0] & [J_{\underline{P}}] \end{bmatrix} \quad (50)$$

$$[K_{yx}] = \begin{bmatrix} [K_{\underline{yx}}] & [K_{\underline{y\theta}}] \\ [K_{\underline{\phi x}}] & [K_{\underline{\phi\theta}}] \end{bmatrix} - \left(\frac{\epsilon}{\sqrt{1+\epsilon^2}} + e\Omega \right) [\tilde{K}_s] - \frac{\dot{\Omega}}{2} \begin{bmatrix} [0] & [0] \\ [0] & [J_{\underline{P}}] \end{bmatrix} \quad (51)$$

$$\{F_x\} = \begin{Bmatrix} \{\mathrm{Me}_u[\Omega^2\cos(\lambda+\alpha) + \dot{\Omega}\sin(\lambda+\alpha)]\} \\ \{\tau(J_P - J_T)[\Omega^2\cos(\lambda+\beta) + \dot{\Omega}\sin(\lambda+\beta)]\} \end{Bmatrix} \quad (52)$$

$$\{F_y\} = \begin{Bmatrix} \{\mathrm{Me}_u[\Omega^2\sin(\lambda+\alpha) - \dot{\Omega}\cos(\lambda+\alpha)]\} \\ \{\tau(J_P - J_T)[\Omega^2\sin(\lambda+\beta) - \dot{\Omega}\cos(\lambda+\beta)]\} \end{Bmatrix} \quad (53)$$

$$\{X\} = \begin{Bmatrix} \{x\} \\ \{\theta\} \end{Bmatrix}; \quad \{y\} = \begin{Bmatrix} \{y\} \\ \{\phi\} \end{Bmatrix} \quad (54)$$

The size of this equation is four times the number of nodes in the rotor model.

Printed in U.S.A.